High-Energy Excitonic Transitions in CdSe Quantum Dots

ARTICLE *in* THE JOURNAL OF PHYSICAL CHEMISTRY B · AUGUST 1998

Impact Factor: 3.3 · DOI: 10.1021/jp981018n

1 AUTHOR:

Alex Zunger
University of Colorado Boulder
768 PUBLICATIONS **50,858** CITATIONS

The Journal of Physical Chemistry B

 VOLUME 102, NUMBER 34, AUGUST 20, 1998

LETTERS

High-Energy Excitonic Transitions in CdSe Quantum Dots

Lin-Wang Wang* and Alex Zunger

National Renewable Energy Laboratory, Golden, Colorado 80401

Received: February 4, 1998; In Final Form: June 16, 1998

An atomistic direct diagonalization pseudopotential approach has been used to analyze the optical excitation spectra of CdSe quantum dots for up to 1.5 eV about the band gap. Good agreement is obtained with experiment for all the eight excitonic transitions, without resorting to fitting to the experimental data on dots. The observed excitonic transitions are identified in terms of specific pairs of valence and conduction single-particle states. For the lowest few transitions, the assignments agree with the conventional k.p effective-mass result, but this is not the case for the higher peaks. Indeed, we find in our atomistic approach that many more valence states exist within a given energy range than in the continuum k.p approach. Furthermore, we find that the mixing of even and odd angular momentum symmetry, disallowed in the contemporary simple k.p models, is actually permitted in the more general atomistic approach.

Semiconductor quantum dots are sometimes referred to as "artificial atoms".[1] Indeed, one of the goals of the theory of quantum dots is to understand the optical spectroscopy at a level of accuracy and detail similar to that underlying atomic physics. The ability to control the laboratory size of the quantum dot, the existence of atomistic features in the potential experienced by the electrons in a quantum dot, and the absence of continuous rotation symmetry even in spherical dots (because of the atomic nature) all make the spectroscopy of quantum dots rich in details and challenging to understand. While most spectroscopic studies of quantum dots have focused on the splitting[2] and red-shift[3] of the *lowest* excitonic transition, interest has recently focused on higher excited states.[4−7] While semiconductor-*embedded* quantum dots (e.g., InAs in GaAs[8] or InP in GaP[9]) exhibit only two to three excitonic transitions, "free-standing" colloidal dots have a narrower size distribution[10] and large electron and hole confinement energies, so that a larger number of excitonic transitions have been resolved.[4,5,8,9] One of the best studied colloidal quantum dots is CdSe,[10] in which as many as 10 excitonic transitions have been detected in size selective photoluminescence excitation (PLE) spectroscopy.[4] This provides rich experimental details and, at the same time, a stringent test for our theoretical understanding of the problem.

Norris and Bawendi[4] analyzed the excitonic spectra of CdSe dots using an effective mass 6×6 k.p model, familiar from the theory of bulk excitons.[11] In this k.p approach, the quantum dot Hamiltonian has both spherical and inversion symmetries. Only the six p-like, bulk states at the top of valence band (HOMO) are used to describe the states of the dot. The Hamiltonian parameters are fitted to the bulk effective masses and, in the cases of ref 4, are further fitted explicitly to the energy levels of the quantum dot. Using this procedure, Norris and Bawendi[4] were able to obtain calculated transition energies that agree well with the observed energies of the absorption peaks. However, as recently shown,[12] if one avoids fitting the theory to the measured data in the quantum dots, the k.p theory results in significantly different predictions for the lowest excitation energy and for the symmetry (s,p) of the near edge states relative to *atomistic* models, such as the direct diagonalization (DD) of the screened pseudopotential Hamiltonian.[15−17] Indeed, for colloidal InP dots, the application[13] of the same 6×6 k.p that was successful in CdSe dots[4] leads to significant discrepancies with experiment,[13] whose explanation required DD

S1089-5647(98)01018-9 CCC: $15.00
Published on Web 08/05/1998

approach.[14] It is thus interesting to revisit CdSe and to study the higher energy excitonic spectra using the same atomistic DD approach. This will examine our theoretical understanding of the system by observing whether agreement with experiment can be obtained without explicitly fitting to the data. This study can also be used as a benchmark for the applicability of the direct diagonalization pseudopotential method and for our detailed understanding of the exciton spectroscopy in a quantum dot.

In the following, we show that, using the direct diagonalization pseudopotential method, one can obtain very good agreement with experiment for as many as eight excitonic transitions. Furthermore, the atomistic theory reveals many surprises when compared with the continuum-type k.p approach. In particular, the direct diagonalization pseudopotential approach (i) gives many more single-particle valence states within the experimentally relevant energy window, (ii) produces different assignment of excitons in terms of pairs of valence states and conduction states, (iii) yields larger averaged total angular momentum F for hole states, and (iv), in contrast with the commonly practiced spherical k.p method, mixes the even and odd angular momentum envelope functions symmetries.

The direct diagonalization of a pseudopotential Hamiltonian method has two steps: the single-particle problem and the electron−hole interaction problem:

(a) *The single-particle problem*: In this first step, we solve the single-particle Schrodinger equation for the wave function $\psi(\mathbf{x})$ [here $\mathbf{x} \equiv (\mathbf{r}, \sigma)$ and where $\sigma = \uparrow, \downarrow$ are the spin variable]:

$$\left\{-\frac{1}{2}\nabla^2 + \sum_{n,\alpha}\hat{v}_\alpha(|\mathbf{r} - \mathbf{R}_{n,\alpha}|)\right\}\psi_i(\mathbf{x}) = \epsilon_i\psi_i(\mathbf{x}) \qquad (1)$$

Here $\hat{v}_\alpha(r)$ is the screened pseudopotential of atom of type α at position $\mathbf{R}_{n,\alpha}$. The pseudopotential $\hat{v}_\alpha(r)$ contains a local part and a nonlocal part that includes spin−orbit interactions. $\hat{v}_\alpha(r)$ was previously obtained by "inverting" the self-consistently calculated ab initio bulk total potentials of CdSe in a few crystal structures and unit cell volumes. This assures that the wave functions have ab initio quality. Furthermore, special attention is directed[16] at obtaining experimentally realistic effective masses and bulk band structures throughout the Brillouin zone. This is particularly important as dot orbitals represent an all-zone superposition of the bulk wave functions.[14] Equation 1 is solved for $\sim 10^3$ atom dots using the linear scaling "folded spectrum method" (FSM),[17] which directly obtains the eigensolutions of the band edge states without having to solve for the many states below the band gap. While the observed CdSe quantum dots have the wurtzite crystal structure, we assume here instead the zince blende structure so as to compare with the k.p results that are under this assumption. Our bulk zince blende pseudopotential calculation has a band gap of 1.835 eV, in agreement (within a few millielectron volts) with the experimental bulk band gap at 10 K. We studied spherical, Se-centered quantum dots of sizes $Cd_{68}Se_{79}$, $Cd_{152}Se_{141}$, $Cd_{312}Se_{321}$, and $Cd_{484}Se_{495}$, with effective diameters of 19.9, 25.0, 32.4, 37.4 Å, respectively. The surface of the quantum dots were passivated with "ligand potentials", which remove all the surface states a few electronvolts away from the band gap.[15] As a result, all the wave functions of our calculated states are extended throughout the interior of the quantum dot (see later Figure 5 for an example), rather than being surface-localized. Our method differs from the ab initio self-consistent calculations (e.g., Hartree−Fock or density functional theory) in that the screened pseudopotential in eq 1 is extracted from the bulk (with appropriate surface effects), rather than iterated self-consistently for the dot. Our calculation differs from the k.p approach in that it permits the dot orbitals to be constructed from an arbitrary superposition of bulk bands throughout the Brillouin zone. Furthermore, the effects of surface and shape are treated atomistically and not perturbatively.

(b) *The electron−hole two-body problem*: In the second step, we calculate the excitonic transition energy

$$E_{i,j} = \epsilon_{j,c} - \epsilon_{i,v} - J_{ij} \qquad (2)$$

where J_{ij} is the Coulomb energy between the electron and holes. Here we have neglected the exchange interaction and correlation effects, which give rise to "fine structure splitting" that will be discussed in another publication, using the many-body expansion approach.[18] J_{ij} is calculated by

$$J_{i,j} = \int\int \frac{|\psi_{i,v}(\mathbf{x}_1)|^2|\psi_{j,c}(\mathbf{x}_2)|^2}{\bar{\epsilon}(\mathbf{r}_1 - \mathbf{r}_2)|\mathbf{r}_1 - \mathbf{r}_2|}\,d^3\mathbf{x}_1 d^3\mathbf{x}_2 \qquad (3)$$

Unlike the case in bulk excitons, here the electron and hole are very close to each other, so a distance-dependent dielectric function $\bar{\epsilon}(\mathbf{r}_1 - \mathbf{r}_2)$ is needed to obtain an accurate description of the Coulomb interaction energy. Using the polaronic model of Haken,[19] the Fourier transform of $\epsilon^{-1}(\mathbf{r}_1 - \mathbf{r})$ [here, $1/\{\bar{\epsilon}(r_1 - r_2)|r_1 - r_2|\} = \int \epsilon^{-1}(r_1 - r)(1/|r - r_2|)\,d^3 r$] can be expressed as $\epsilon^{-1}(\mathbf{k}) = \epsilon_{el}^{-1}(k) + \Delta\epsilon_{ion}^{-1}(k)$, containing the electronic (el) and ionic (ion) contributions, respectively. Using the Thomas−Fermi model of Resta,[20] these two terms have the analytical forms of

$$\epsilon_{el}^{-1}(k) = \frac{k^2 + q^2\sin(kR_\infty)/(\epsilon_\infty^{dot}\,kR_\infty)}{k^2 + q^2} \qquad (4)$$

$$\Delta\epsilon_{ion}^{-1}(k) = \left(\frac{1}{\epsilon_0^{dot}} - \frac{1}{\epsilon_\infty^{dot}}\right)\left(\frac{1/2}{1 + \rho_h^2 k^2} + \frac{1/2}{1 + \rho_e^2 k^2}\right) \qquad (5)$$

Here $\rho_{h,e} = (2m_{h,e}^*\omega_{LO}/\hbar)^{-1/2}$, and ω_{LO} is the longitudinal optical-phonon frequency and m_e^* and m_h^* are electron and hole effective masses, respectively. In eq 4, $q = 2\pi^{-1/2}\,(3\pi^2 n_0)^{1/3}$ (where n_0 is the electron density), and R_∞ is the solution of the equation $\sinh(qR_\infty)/(qR_\infty) = \epsilon_\infty^{dot}$. Also, $\epsilon_0^{dot} = \epsilon_\infty^{dot} + \Delta\epsilon_{ion}$ and $\Delta\epsilon_{ion} = 3.5$ for CdSe derived from the bulk. ϵ_∞^{dot} is calculated in ref 15. The resulting ϵ_∞^{dot} used for the current four quantum dots (from small size to large size) are 4.87, 5.10, 5.38, 5.54, respectively (the bulk value is $\epsilon_\infty^{bulk} = 6.2$). The Coulomb energies calculated from eq 3 range from 150 to 400 meV, and, usually, the higher energy excitons have smaller Coulomb energies. If one uses instead the standard effective mass formula[21] to calculate the Coulomb energy (with a constant $\epsilon_0^{bulk} = 9.7$), one finds that J_{ij} ranges from 140 to 260 meV, and the variation of J_{ij} for different pairs of $\psi_{i,v}$ and $\psi_{j,c}$ are smaller than what eq 3 gives. These are significant errors, avoided here by calculating J_{ij} explicitly for each i and j pair.

Once the excitonic energies $E_{i,j}$ are calculated, the transition probability I_{ij} for each electron−hold pair is obtained via the Fermi Golden rule: $I_{ij} = 4e^2E_{i,j}|\langle\psi_{i,v}|\nabla|\psi_{j,c}\rangle|^2/3m^2c^3$, where m is the electron mass and c is the speed of light. The optical absorption spectrum is obtained by a 25 meV broadening of each transition peak, i.e., $I(E) = \sum_{ij} I_{ij} f(E - E_{ij})$, where $f(E - E_{ij})$ is the broadening function. In summing over ij, we calculated 40 single-particle valence states (80, counting the Kramer's doubling) and 10 (20 with Kramer's doubling)

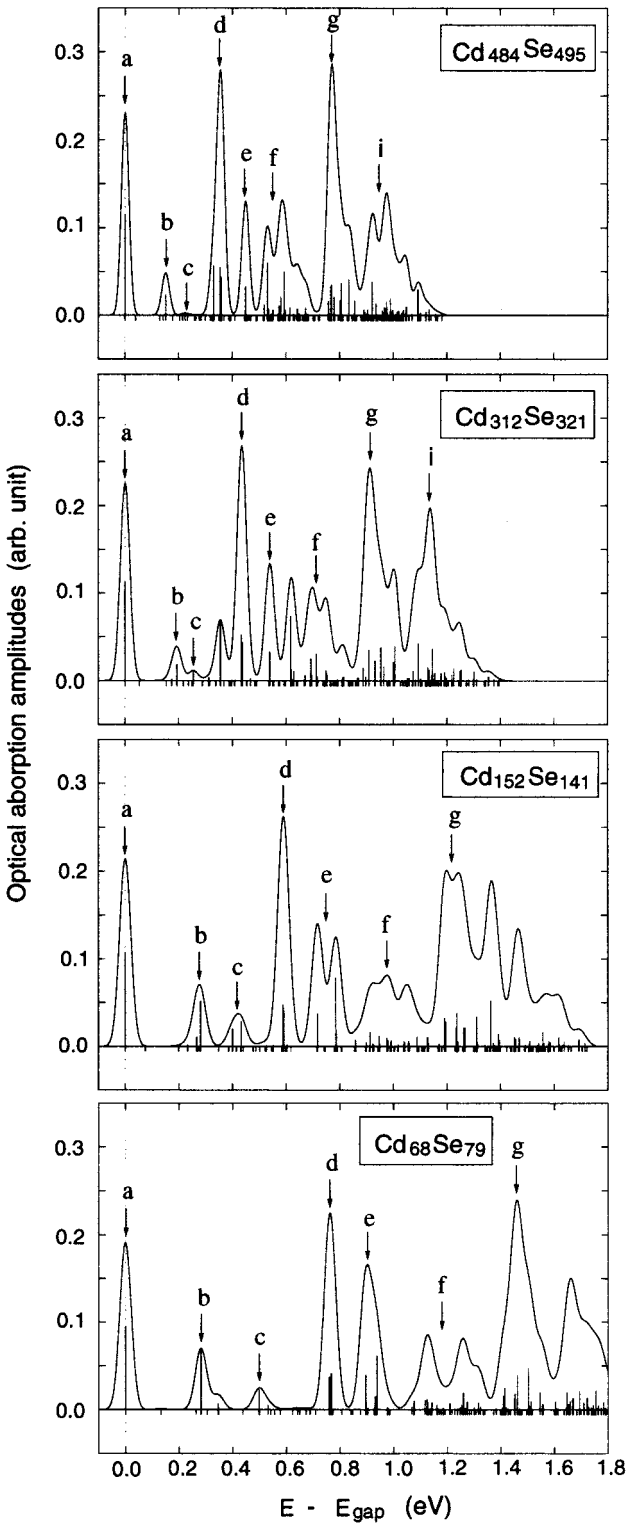

Figure 1. Optical transition spectra of spherical zince blende CdSe dots calculated using the screened pseudopotential Hamiltonian. Arrows point to the main peaks. The short vertical negative bars denote the transition energies $E_{i,j}$ of eq 2, and the vertical positive bars denote the magnitudes of the transition matrix elements.

conduction states, covering a E_{ij} range of ~1.4 eV. The resulting $I(E)$'s are shown in Figure 1, where the short vertical negative bars denote the excitonic transition energies $E_{i,j}$ of eq 2, while the positive bars indicate the matrix elements $|\langle\psi_{i,v}|\nabla|\psi_{j,c}\rangle|^2$ for each transition.

We next identify the major transition peaks and assign indices a−i to them (arrows in Figure 1). The assignment is done by considering the line shapes and intensity of the transition peaks and a consistent trend from the small to large quantum dots. Thus, each major peak might contain a few closely spaced small peaks. For the cases where there is no obvious peak position, the center of mass of the major peak is used as the position of the peak. There is some uncertainty in assigning the peak positions, especially in the higher energy part of the spectrum, i.e., peaks f, g, and i. Indeed, had we based our assignments on the spectrum of a single-size dot alone in Figure 1, this uncertainty could have been as large as the separation between the peaks. However, we based our assignments on the observation of the development of peaks as the dot size varies. Consequently, as can be seen in Figure 1, this uncertainty is much reduced. Notice that we have used the full optical spectra to assign the peaks. This is more reliable (especially for the higher energy peaks) than assigning peak positions according to transition energies only.[4]

Before comparing with experiment, we note that the experimental data in Figure 4 of ref 4 contains the effect of phonon replica, exchange splitting, and crystal field splitting, which are not considered in our (or in the k.p) calculations.[18] To subtract these fine-structure effects from the data, we have used the fine structure model of ref 2. On the basis of this model, we calculate from ref 2 a new band gap E_{gap}, which corresponds to the lowest excitation energy E_a in the absence of the exchange splitting and crystal field splitting. The experimental data in Figure 4 of ref 4 is replotted in Figure 2 using this new definition of E_a (see footnote 22 for a more detailed descriptions of this procedure). We also plotted the calculated relative peak energies $E_i - E_a$ ($i = a$ to i) as a function of the effective gap E_a in Figure 2a.

Overall, Figure 2 shows that the present calculation is in very good agreement with experiment. However, not all of the observed transition peaks are accounted for: (1) Our calculation here is limited to dots with $E_{gap} > 2.1$ eV. Dots with smaller band gaps correspond to dot size $\gg$ 1000 atoms that are not calculated here. (2) The energy of the experimental peak j is beyond the energy range of our calculation; thus, there is no corresponding calculated value for it. (3) The experimental peak h is weak and very close to g. Furthermore, it is in the high-energy range of our spectrum, where many small peaks exist. Thus, without analyzing all these details, and without doing an ensemble averages over the different shapes, we do not feel confident to assign such a peak. (4) At the large E_{gap} value (small quantum dot size), experiment does not find peak c at the calculated energy. This is not fully understood at this time and remains to be investigated in the future. One complication is that there is another peak (i.e., the peak between c and d in the $Cd_{312}Se_{321}$ panel of Figure 1), which moves from d to b when the quantum dot size is reduced from $Cd_{484}Se_{495}$ to $Cd_{68}Se_{79}$. Better experimental data (e.g., single-dot spectra) are needed to analyze such fine details.

Around $E_{gap} \sim 2.0$ eV, which is outside the range of the present ~1000 atom calculations, the data shows an interesting anticrossing between peaks g and e. This can be explained, however, via a simple model. The anticrossing involves two states, labeled α and β: (α) a low quantum number state derived from the split-off bulk band (which approaches $E_i - E_{gap} = 0.42$ eV at the bulk E_{gap} of 1.84 eV) and (β) a high quantum number state derived from the heavy hole and light hole bulk bands (which approaches $E_i - E_{gap} = 0$ eV at the bulk E_{gap} of 1.84 eV). The occurrence of the anticrossing is thus expected because the energy of state α should rise slower as E_{gap} increases (smaller dot size) than the energy of state β. This model and

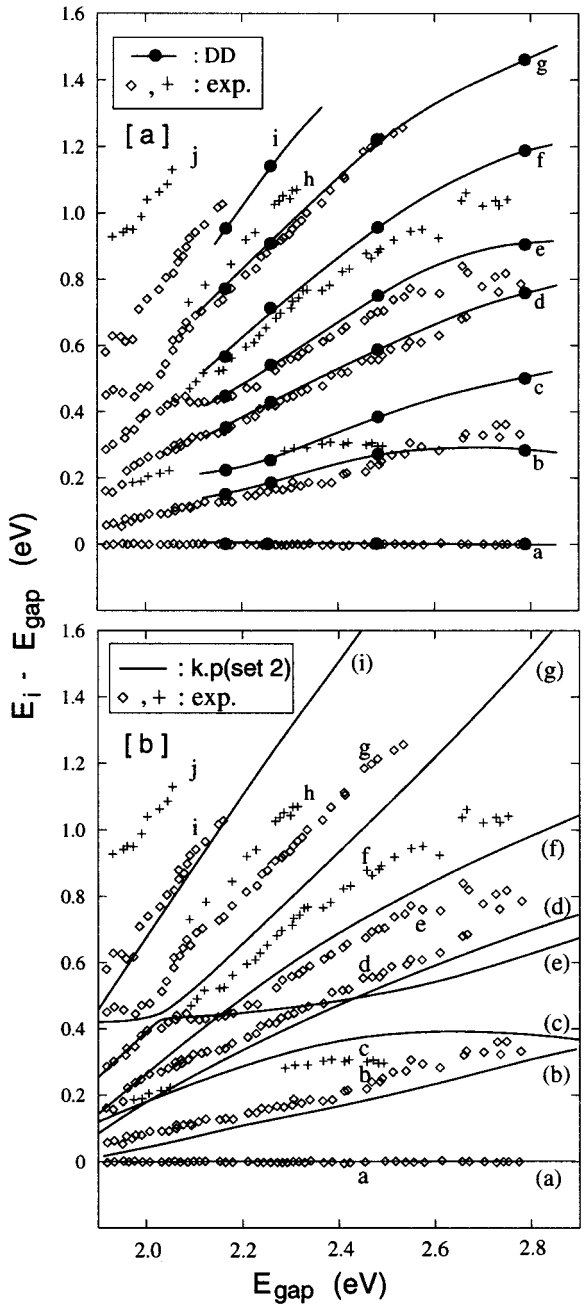

Figure 2. Transition energies in spherical zince blende CdSe dots (relative to the first excited state) vs the energy of the first excited state (effective band gap). The experimental data are taken from ref 4, after removal of the exchange and crystal field effects.[22] In (a), the direct diagonalization peaks in Figure 1 are plotted as filled circles. In (b), the k.p curves are copied from ref 4 without change. The letters in parentheses (a−i) in (b) denote the k.p transitions, and the unbracketed letters a−i are for the experimental results.

the appearance of the crossing remain to be tested by our direct diagonalization method in the future.

In Figure 2b, we have copied the k.p result of ref 4 to compare with the adjusted[22] experimental data. Thus, the same correction is applied to the experimental data as they are compared to the direct diagonalization results and the k.p results. As we can see, the k.p transitions labeled (a), (b) and (d), which were explicitly fitted to the raw experimental data, still agree well with the adjusted[22] experimental results. However, the k.p energy for the other transitions are shifted away from the experimental peaks. Notably, the k.p transition energy (e) is too low for large E_{gap}, and the k.p transition (f) is closer to the

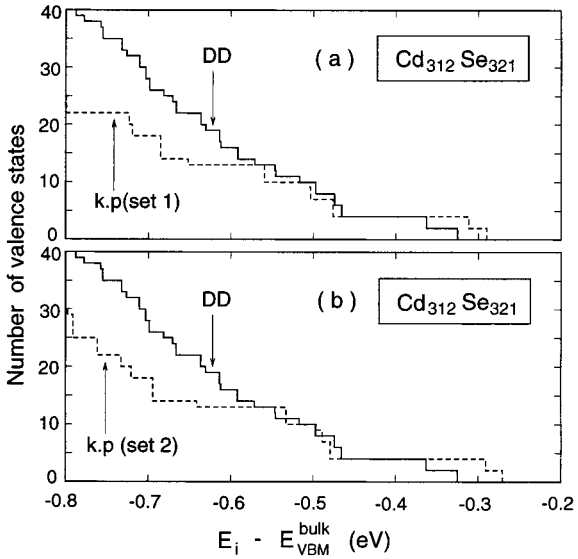

Figure 3. Accumulated number of valence states starting from the top of valence band. The parameters ($\gamma_1 = 2.52$, $\bar{\gamma} = 0.83$, $\Delta_0 = 0.42$ eV) of the 6 × 6 k.p (set 1) are derived from DD bulk band structure, and the parameters ($\bar{\gamma}_1 = 2.04$, $\bar{\gamma} = 0.58$, $\Delta_0 = 0.42$) of the 6 × 6 k.p (set 2) are taken from ref 4.

experimental peak e than to f. Note that the direct diagonalization pseudopotential results without fitting are closer to experiment than the explicitly fitted k.p results.

Some inconsistency of the k.p model with experiment is reflected in the relative peak intensity in the optical spectra. In ref 23, it was shown that in the k.p model for CdSe, peak c is stronger than peak b. However, experimentally,[23] peak b is stronger than peak c. This feature is reproduced correctly by our results in Figure 1. Indeed, for the higher energy peaks e−i, the k.p model used only the positions of the energy levels (rather than their intensity) to establish the assignments. Here, we base the spectroscopic assignment on the spectral shape of Figure 1, in the same way as the experimental peaks are derived. The interpretation is thus more robust.

The difference between direct diagonalization pseudopotential results and the k.p results in Figure 2 has two sources: one is due to differences in the single particle energies ϵ_i (eq 1), and the other is due to differences in the Coulomb energy J_{ij} (eq 3). The Coulomb energy difference can cause a ∼50 meV overall shift for the positions of higher energy peaks. However, the major difference between the k.p results and the direct diagonalization pseudopotential results comes from the difference in the single-particle energy ϵ_i. In Figure 3, we have plotted the number of single-particle valence states starting from the top of valence band. We use the k.p parameters of Norris and Bawendi[4] ("set 2") as well as the parameters extracted from the bulk pseudopotential band structure of CdSe ("set 1").[12] The k.p energy levels are calculated using the formalism of ref 11. *We see that there are almost twice as many states in the atomistic calculation than in the continuum k.p calculation within the same energy range.* To understand this surprising difference, we have compared the angular momenta of the envelope functions of the k.p and the direct diagonalization pseudopotential wave functions (Figure 4). This figure shows the energies of the individual single-particle valence states within the energy range studied. The k.p states are labeled as follows: the first number is the principle quantum number; the capital letters before "-" denote the angular momenta L of the envelope functions of the heavy and light hole bands; the capital letter after "-" is the angular momentum of the split-off band;

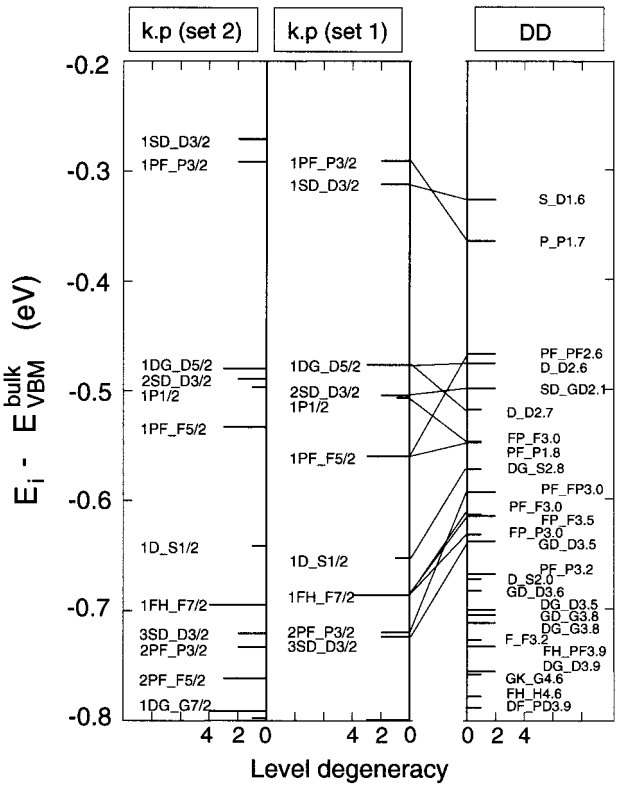

Figure 4. Valence state analysis of the $Cd_{312}Se_{321}$ quantum dot. See caption of Figure 3 for the definition of k.p (set 1) and k.p (set 2). The length of the bar indicates the degeneracy (without counting the Kramer's doubling).

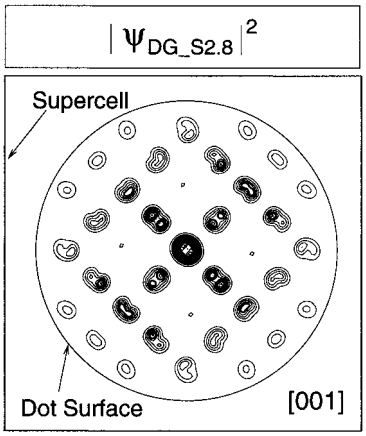

Figure 5. Wave function charge density contour plot of DD state $\psi_{DG\_S2.8}$ of the $Cd_{312}Se_{321}$ quantum dot on a [001] cross section.

the final half-integer is the total angular momentum F. We have similarly decomposed our directly diagonalized wave functions $\psi_{i,v}(\mathbf{x})$ into k.p-style envelope functions

$$\psi_{i,v}(\mathbf{x}) = \sum_n u_n(\mathbf{x})\, f_n(\mathbf{r}) = \sum_n u_n(\mathbf{x})\, [\sum_{L,m} f_n^{L,m}(|\mathbf{r}|) Y_{L,m}(\theta, \phi)] \tag{6}$$

where $u_n(\mathbf{x})$ is the nth band *bulk* Bloch function at the Γ point ($\mathbf{k} = 0$), $f_n(\mathbf{r})$ is the corresponding envelope function, and $Y_{L,m}(\theta, \phi)$ is the spherical harmonics of angular momentum L. The total integrated weight of $\sum_{m=-L,L} |f_n^{L,m}(|\mathbf{r}|)|^2$ for each $\{n, L\}$ is denoted as $w_{n,L}$. We have used the heavy hole, light hole, and split-off bands for n, and the total weights on these bands $\sum_{L,n=3-8} w_{n,L}$ is around ~0.9. Figure 4 depicts the dominant weights $w_{n,L}$ of each single-particle state: The capital letter

TABLE 1: Assignments of the Excitonic Transition Peaks in the $Cd_{312}Se_{321}$ Quantum Dot to Pairs of Hole and Electron States[a]

transition	DD valence → conduction	k.p (set 2) valence → conduction
a	(1−2)S_D1.6 → (1)S_e	1SD_D3/2 → 1S_e
b	(9−10)SD_GD2.1 → (1)S_e	2SD_D3/2 → 1S_e
c	(14)DG_S2.8 → (1)S_e	1D_S1/2 → 1S_e
d	(3−4)P_P1.7 → (2−4)P_e	1PF_P3/2 → 1P_e
e	(5−6)PF_PF2.6 → (3−4)P_e	2D_S1/2 → 1S_e
f	(17)PF_F3.0 → (2−4)P_e (20)FP_P3.0 → (2−4)P_e (23−24)PF_P3.2 → (2−4)P_e	1PF_F5/2 → 1P_e 1P1/2 → 1P_e
g	(7−8)D_D2.6 → (5−7)D_e (9−10)SD_GD2.1 → (5−6)D_e (11)D_D2.7 → (7)D_e (7−8)D_D2.6 → (8−9)D_e	3D_S1/2 → 1S_e

[a] The numbers in the bracket of the direct diagonalization (DD) assignments are the running indices of the valence (conduction) states counted from the top of valence band (bottom of conduction band).

before "-" indicates those angular momenta L's whose sum of $w_{n,L}$ on the heavy hole and light hole bands are larger than 0.1. The L's are in descending order according to their weights. The letter after "-" indicates the highest weight angular momentum L for the split-off band. The last number is an averaged total angular momentum F, calculated as

$$F(F+1) = \langle \sum_n u_n f_n | (\hat{F}_u + \hat{F}_f)^2 | \sum_m u_m f_m \rangle \tag{7}$$

Here the angular momentum operator $\hat{F}_u = i\mathbf{r} \times \nabla + \vec{s}$, ($\vec{s}$ is the Dirac spin matrix) applies only to u_n, and $\hat{F}_f = i\mathbf{r} \times \nabla$ applies only to f_n.

In analyzing the results, we note that unlike the spherical k.p model, the atomistic Hamiltonian we use has the T_d point group symmetry. Consequently, the largest degeneracy of the direct diagonalization state is only 2, while in k.p, the degeneracy is $(2F + 1)/2$. We have made a tentative connection in Figure 4 between the DD and k.p states to indicate how does each k.p state breaks down into DD states. Our conclusions are:

(i) The averaged F for a given direct diagonalization state is usually significantly larger than its k.p counterpart. This is due to the existence of high L components (allowed because the F is no longer a good quantum number) in the DD envelope function.

(ii) Owing to the lack of inversion symmetry in T_d, the even and odd L envelope functions can coexist in $w_{n,L}$ for the same band n, while in the spherical 6 × 6 k.p model, the envelope functions are either even or odd.

(iii) The k.p model uses a parabolic bulk band dispersion, which deviates from the exact bulk band structure when the k vector shifts away from the $k = 0$ Γ point. As a result, the energy difference between k.p and DD dot eigenstates increases for higher quantum number states (which correspond to larger k point values). This trend is evident in Figure 4. As a result, the k.p states that correspond to the DD "extra states" have energies outside the range of Figure 4. This leads to a smaller number of k.p states (Figure 3) within the experimentally relevant energy window.

(iv) The quantitative features of the connected k.p and DD states in Figure 4 can be very different. This is manifested by their value of F, the weights $w_{n,L}$, and the real space shape of the wave function. For example, Figure 5 shows the contour

plot of the DD wave function DG_D2.8. Its envelope function shows orientational preferences in the (110) and (1$\bar{1}$0) directions. On the other hand, the corresponding k.p state 1D_S1/2 is spherically symmetric.

Table 1 compares the assignments of the absorption peaks (in terms of pairs of valence states and conduction states) between the k.p model and DD approach. The same assignments are achieved for the lowest energy peaks a−d, but not for the higher energy peaks e−g. For peak f, the conduction state assignments are the same, but the valence states are different. For peaks e and g, both the conduction-state and valence-state assignments are different. To explain the higher energy absorption peaks (e.g., g), the k.p model relies on the lowest conduction states $1S_e$, $1P_e$, and on the very deep valence states (e.g., 2D_S1/2, 3D_S1/2). On the other hand, in the DD approach, the higher energy transitions originate both from the shallow valence states and from the higher conduction states (D_e). This different assignment also explains the roles of the "extra" DD states (compared to k.p results, Figure 3) in the optical transition: combined with higher conduction states, these extra valence states form the higher energy transitions, thus providing a different interpretation than the k.p assignment. Finally, our calculated electron s and p state energy splittings agree well with the experimental results[24] if the s−p splitting is plotted as a function of E_{gap} as in Figure 2.

In summary, we have shown that an atomistic direct-diagonalization pseudopotential approach can be used to explain the energies, intensities, and symmetries of as many as eight excitonic transition peaks in CdSe dots. We have identified the observed excitons in terms of specific pairs of valence and conduction orbitals. The results differ from conventional k.p method in a number of important ways:

(1) The Coulomb energies have a strong dependence on the orbitals of the electron and the hole. This is neglected in standard effective mass treatment.

(2) Considering the top 1 eV below the HOMO, there are many more valence energy levels in the atomistic pseudopotential approach than in the continuum k.p approach (Figures 3 and 4).

(3) The spatial anisotropy of k.p and pseudopotential wave function is very different (Figure 5).

(4) The relative intensities of peaks c and b are inverted in k.p results relative to pseudopotential calculations and experiments.

(5) The average angular momentum F is larger in the atomistic approach than in k.p approach (Table 1).

(6) The atomistic approach shows significant mixing of even and odd angular momentum envelope function symmetries, which is not allowed in the spherical k.p approach.

(7) Last, the energy peak positions in Figure 2 given by the atomistic approach are different from the k.p results and compare better with the experiment than the explicitly fitted k.p results.

Acknowledgment. We thank D. J. Norris and M. G. Bawendi for discussions on the subject. This work was supported by the Office of Energy Research, Material Science Division, U.S. Department of Energy, under Grant No. DE-AC02-83CH10093.

References and Notes

(1) Ashoori, R. C. *Nature* **1996**, *379*, 413.
(2) Norris, D. J.; Efros, Al. L.; Rosen, M.; Bawendi, M. G. *Phys. Rev. B* **1996**, *53*, 16347.
(3) Micic, O. I.; Cheong, H. M.; Fu, H.; Zunger, A.; Sprague, J. R.; Mascarenhas, A.; Nozik, A. J.; *J. Phys. Chem.* **1997**, *101*, 4904.
(4) Norris, D. J.; Bawendi, M. G. *Phys. Rev. B* **1996**, *53*, 16338.
(5) Masumoto, Y.; Sonobe, K. *Phys. Rev. B* **1997**, *56*, 9734.
(6) Bertram, D.; Micic, O. I.; Nozik, A. J. *Phys. Rev. B* **1998**, *57*, R4265.
(7) Banin, U.; Lee, J. C.; Guzelian, A. A.; Kadavanich, A. V.; Alivisatos, A. P.; Jaskolski, W.; Bryant, G. W.; Efros, Al. L.; Rosen, M. Unpublished.
(8) Ruvimov, S.; Werner, P.; Scheerschmidt, K.; Gosele, U.; Heydenreich, J.; Richter, U.; Ledentsov, N. N.; Grundmann, M.; Bimberg, D.; Ustinov, V. M.; Egorov, A. Y.; Kop'ev, P. S.; Alferov, Zh. I. *Phys. Rev. B* **1995**, *51*, 14766.
(9) Hessman, D.; Castrillo, P.; Pistol, M.-E.; Pryor, C.; Samuelsum, L. *Appl. Phys. Lett.* **1996**, *69*, 749.
(10) Murray, C. B.; Norris, D. J.; Bawendi, M. G. *J. Am. Chem. Soc.* **1993**, *115*, 8706.
(11) Ekimov, A. I.; Hache, F.; Schanne-Klein, M. C.; Richard, D.; Flytzanis, C.; Kudryavtsev, I. A.; Yazeva, T. V.; Rodina, A. V.; Efros, Al. L. *J. Opt. Soc. Am. B* **1993**, *10*, 100.
(12) Fu, H.; Wang, L. W.; Zunger, A. *Appl. Phys. Lett.* **1997**, *71*, 3433. *Ibid. Phys. Rev. B* **1998**, *57*, 9971.
(13) Betram, D.; Micic, O. I.; Nozik, A. J. *Phys. Rev. B* **1998**, *57*, R4265.
(14) Fu, H.; Zunger, A. *Phys. Rev. B* **1998**, *57*, R15064.
(15) Wang, L. W.; Zunger, A. *Phys. Rev. B* **1996**, *53*, 9579.
(16) Wang, L. W.; Zunger, A. *Phys. Rev. B* **1995**, *51*, 17398.
(17) Wang, L. W.; Zunger, A. *J. Chem. Phys.* **1994**, *100*, 2394.
(18) Franceshetti, A.; Wang, L. W.; Fu, H.; Zunger, A. Unpublished. Zunger, A. *MRS Bull.* **1998**, *23* (2), 35.
(19) Haken, H. *Nuovo Cimento* **1956**, *10*, 1230.
(20) Resta, R. *Phys. Rev. B* **1977**, *16*, 2717.
(21) Brus, L. E. *J. Phys. Chem.* **1986**, *90*, 2555.
(22) Exchange and crystal field combine to split the first transition to levels denoted in ref 2 as $2,1^L$, 0^U and 1^U. The measured energies include: the PLE detection energy, peak α (denoted δ_1 in Table 1 of ref 2), and peak β (denoted δ_2,δ_3 in their Table 1). If we assign the detection energy to level 2, peak α to level 1^L, and peak β to levels 0^U and 1^U, then by solving the model of ref 2, we get the effective energy gap corresponding to the removal of the exchange interaction and phonon replicas: $E_{gap} \simeq E_\beta - 0.04(E_\beta - 1.75)$ (eV). In their original plot (Figure 4 of ref 4), the authors used E_β as the energy band gap. We have corrected this here in Figure 2.
(23) Schmidt, M. E.; Blanton, S. A.; Hines, M. A.; Guyot-Sionnest, P. *Phys. Rev. B* **1996**, *53*, 12629.
(24) Guyot-Sionnest, P.; Hines, M. A. *Appl. Phys. Lett.* **1998**, *72*, 686.